Lithography-free fabrication of scalable 3D nanopillars as ultrasensitive SERS substrates

Chirumamilla, Anisha; Moise, Ioana Malina; Cai, Ziru; Ding, Fei; Jensen, Karina B.; Wang, Deyong; Kristensen, Peter K.; Jensen, Lars R.; Fojan, Peter; Popok, Vladimir; Chirumamilla, Manohar; Pedersen, Kjeld

Published in:
Applied Materials Today

DOI (link to publication from Publisher):
10.1016/j.apmt.2023.101763

Publication date:
2023

Document Version
Publisher's PDF, also known as Version of record

Applied Materials Today 31 (2023) 101763

Contents lists available at ScienceDirect

Applied Materials Today

journal homepage: www.elsevier.com/locate/apmt

Lithography-free fabrication of scalable 3D nanopillars as ultrasensitive SERS substrates

Anisha Chirumamilla [a,*], Ioana-Malina Moise [a], Ziru Cai [b], Fei Ding [b], Karina B. Jensen [a], Deyong Wang [a], Peter K. Kristensen [a], Lars R. Jensen [a], Peter Fojan [a], Vladimir Popok [a], Manohar Chirumamilla [a,*], Kjeld Pedersen [a]

[a] Department of Materials and Production, Aalborg University, Skjernvej 4A, Aalborg 9220, Denmark
[b] Centre for Nano Optics, University of Southern Denmark, Campusvej 55, Odense 5230, Denmark

ARTICLE INFO

Keywords:
One-step nanofabrication
3D nanopillars
Large-area plasmonic substrates
Gap plasmon resonator
Surface-enhanced Raman spectroscopy

ABSTRACT

Surface-enhanced Raman spectroscopy (SERS) detection of analyte molecules at ultra-low concentrations requires highly-efficient plasmonic nanostructures enabling a high hot-spot density. However, a facile and cost-effective strategy toward large-area fabrication of efficient nanostructures with significant electromagnetic field enhancement remains a great challenge. Further, SERS faces reliability issues with the molecular fingerprint at ultra-low concentrations. This work shows a one-step rapid fabrication technique utilizing glancing angle deposition for growing 3D nanopillars of Ag or Au, which is facile, scalable and cost-effective. The 3D nanopillar substrates can reliably detect analyte molecules with concentrations as low as 10^{-18} M with a high signal-to-noise ratio molecular fingerprint proven for Cresyl violet, p-aminothiophenol and Rhodamine 6G. The ultra-high enhancement is realized in conjunction with the formation of a high hot-spot density due to localized surface plasmons and surface plasmons at metal/air interface. A portable handheld Raman spectrometer is used to evaluate the potential application of the nanopillars for on-site diagnostics. It avoids the need for sophisticated tabletop instruments yet provides high-precision molecular specificity outside specialized laboratories. The 3D nanopillar substrates show excellent molecular detection limits at 10^{-15} M concentrations when tested with a handheld Raman spectrometer. The uniqueness of the 3D nanopillar features with the formation of a high density of hot-spots and one-step nanofabrication methods provide a platform to unravel on-site diagnostics with cost-effective approaches.

1. Introduction

Large-area fabrication of nanostructures providing highly efficient localized surface-plasmon resonances (LSPRs) shows paramount importance in various applications, such as surface-enhanced Raman spectroscopy (SERS) [1,2], solar absorbers [3,4], thermal emitters [5,6], photodetectors and bio/chemical sensors [7–12]. Particularly SERS, as a label-free detection technique, identifies biological/chemical substances at ultra-low concentrations down to the single molecule level with molecular fingerprints. The low Raman scattering cross-section of the molecules is significantly enhanced by many orders of magnitude when the molecules are placed in the close vicinity of the strong electromagnetic (EM) field of the interacting plasmonic nanostructures, which are called hot-spots [13–15]. SERS enhancement is proportional to the quadrant of local EM field intensity [16,17], where an enhancement factor of 10^{12} is reasonably attainable [18]. Thus, the key parameter to obtain considerable SERS enhancement is fabricating the plasmonic nanostructure arrays enabling hot-spots and tunable LSPR to match the incoming laser excitation.

A wide variety of nanostructures and fabrication methods have been explored for SERS so far [19–28]; however, large-area and low-cost fabrication approaches with minimum fabrication steps are still missing for highly efficient nanostructures enabling them to provide a large density of hot-spots. Usually, Au and Ag-based nanostructures are used [29], where Au-based matrices are eminently stable but expensive and typically offer lower SERS enhancement than Ag counterparts. However, one of the main drawbacks of Ag is functional degradation in ambient air [30], which will decrease the SERS enhancement over the

* Corresponding authors.
E-mail addresses: anishac@mp.aau.dk (A. Chirumamilla), mch@mp.aau.dk (M. Chirumamilla).

https://doi.org/10.1016/j.apmt.2023.101763
Received 27 October 2022; Received in revised form 23 January 2023; Accepted 3 February 2023
Available online 10 February 2023

long term.

Conventional tabletop Raman spectrometers provide molecular-specific information at ultra-low concentrations with high sensitivity. Nevertheless, the necessity of expensive and sophisticated instrumentation with a large device footprint limits their on-site applications in point-of-care diagnostics [31]. Therefore, it is crucial to fabricate nanostructures that can provide the analyte fingerprint with excellent specificity and, at the same time, detection of the molecules at ultra-low concentrations using handheld (portable) Raman spectrometers.

Various one-step nanofabrication routes, such as laser ablation [32–34] and thermal dewetting [35–37] methods, can generate metallic nanopatterns over a large area with a high hot-spot density; however, the SERS signal uniformity is questionable. Glancing angle deposition (GLAD) technique [38–46] provides a selective growth of nanoparticles onto planar/patterned substrates utilizing the shadow effect. 3D nanostructures grown by the GLAD provide a simple route where the SERS signal intensity will be increased by decreasing the nanostructure diameter. Heretofore, the minimum diameter of the linear 3D nanostructures obtained by such a technique has been ~100 nm [47–53].

This work describes an innovative approach for fabricating 3D nanopillars of 40 nm diameter and length up to 350 nm, resulting in analyte molecule detection at ultra-low concentrations of atto molar level, i.e. approaching a single molecule recognition. Herein, we report on the engineering of 3D plasmonic nanopillars comprised of Ag or Au grown by an oblique angle deposition method and using the shadowing effect. The oblique angle deposition method provides freedom for designing complex 3D nanostructures with defined diameter, shape, spacing and density by adjusting deposition rate, incident angle and substrate temperature, and it eliminates the need for post- and pre-processes such as etching and lithography. 3D nanostructures provide a high density of hot-spots as well as a significant number of binding sites for probing analyte molecules within the sampling area [20, 54–57]. The versatility of these Ag nanopillars is tested with various molecules (Cresyl Violet (CV), Rhodamine 6G (R6G) and p-aminothiophenol (p-MA)), and the ultra-sensitivity is demonstrated with p-MA molecules at low concentrations down to 10^{-18} M level. 3D nanopillar substrates also show excellent uniformity of the SERS signals across large areas, making them ideal candidates for bio/chemical sensing applications. Moreover, for the first time, we demonstrate that using a handheld Raman spectrometer, it is possible to detect the analyte molecules at ultra-low concentrations, down to a single molecule regime.

2. Material and methods

2.1. 3D Ag and Au nanostructure fabrication

3D nanostructures were grown by a custom-designed thermal evaporation system, onto 2 × 2 cm^2 substrates cut from Si (100) wafers. The substrates were left with their natural oxide, cleaned by ultrasound in baths of acetone and ethanol, and dried with N_2. A custom-built vacuum system with a base pressure below 10^{-6} mbar is used, and a deposition rate in the range of 0.8 – 1.5 Å/s for Ag and 2.0 – 2.5 Å/s for Au is maintained with the help of a quartz crystal oscillator. The substrate was placed at 85° glancing angle with respect to the metal beam to obtain tilted 3D nanopillar arrays. All presented SEM images are obtained using a Zeiss 1540 XB machine.

2.2. Reflectivity measurements

Reflectivity spectra of the 3D nanopillar structures in the UV and visible range are measured using a PerkinElmer Lambda 1050 spectrometer equipped with a 150 mm integrating sphere where the minimum angle of light incidence is 8°. Reflectivity measurements are performed in the optical range between 300 and 800 nm with a wavelength scan step of 2 nm, where a labsphere spectralon reflectance standard is used for normalization. To investigate the polarization-dependent reflectivity spectra, Glan-Taylor air-spaced polarizers are used.

2.3. Finite-difference time-domain simulations

Optical properties (far- and near-field) of the 3D Ag nanopillars were simulated using a commercial software (FDTD Solution, Lumerical Inc., Vancouver, Canada). A 5 nm mesh grid size is used all over the simulation region, and the incident plane wave source is polarized along the *x*- and y- directions. Periodic boundary conditions are used along the *x*- and y- directions, while PML boundary condition is applied along the *z*-direction.

2.4. X-ray photoelectron spectroscopy (XPS) measurements

XPS was carried out in ultra-high vacuum by PHOIBOS 150 analyser from SPECS utilizing X-rays produced by Mg anode. The pass energy was fixed to 50 eV and to 25 eV for the collection of entire spectrum and smaller energy intervals related to individual chemical elements, respectively. Such approach ensured a high transmission and optimized sensitivity for the identification of doublets and shifts. The samples with Ag nanopillars were measured immediately after the fabrication as well as after 1, 5 and 180 days kept in ambient atmosphere in order to study the chemical changes.

2.5. SERS measurements

SERS measurements were performed by Renishaw inVia micro-Raman spectrometer using a 100 × LEICA objective lens (numerical aperture, NA=0.9), a laser with excitation at 532 nm, and a thermo-electrically cooled charge-coupled device (CCD) as the detector. The instrument was calibrated with respect to the first-order silicon phonon peak at 520 cm^{-1}, and all the spectra were acquired at room temperature in back-scattering geometry. The polarization of the excitation laser source was set parallel to the x-axis unless otherwise specified. The spectra were baseline corrected with a third-order polynomial using Wire 3.4 software.

2.6. Handheld Raman spectroscopy

Raman measurements were acquired with a Bravo handheld Raman spectrometer (Bruker) and controlled using OPUS spectroscopy software. This device is equipped with a Duo laser system (wavelengths of 785 nm and 853 nm), recording the spectrum in two spectral ranges, between 300 and 2200 cm^{-1} and 1200–3200 cm^{-1}, where it provides a better overlap in the spectral range of 1200 and 2200 cm^{-1}. Raman spectra are recorded in the spectral range using 32 accumulations. A polystyrene standard is used prior to the measurements to ensure the device's operation. The laser power at the sample is 45 mW, which is measured using a power meter from Thorlabs.

2.7. Analyte molecule deposition using chemisorption

Different analyte molecules were deposited on the 3D nanostructures by chemisorption method using various concentrations ranging from 1 μM down to 1 aM level. For p-MA, the base solution was prepared by dissolving the p-MA molecule in ethanol, whereas R6G and CV were prepared using deionized water. Then, nanopillar structures were dipped in analyte solution for 20 min for the concentration levels of 1 μM, 1 nM and 1 pM, while for 24 h in the case of 1 fM and 1 aM concentrations, and then rinsed with either ethanol (p-MA) or deionized water (R6G and CV) to remove the excess molecules that are not adsorbed to the metallic surfaces. Afterwards, the nanostructures were dried with gas nitrogen flow. The analyte molecules, p-MA, R6G and CV, employed in this study were purchased from Sigma-Aldrich.

3. Results and discussion

3.1. Design, fabrication and ultra-sensitive SERS detection using Ag nanopillars

A schematic presentation of the 3D Ag nanopillar structures is shown in Fig. 1(a), where *D, L* and α denote the diameter, length and tilt of the nanopillar, respectively. Silver deposition was carried out at an oblique angle of 85°, leading to the growth of nanopillars with α of 62° and *L* up to 350 nm. After increasing the length above 350 nm, mergings of individual nanopillars were observed. A normal-incidence SEM image of the nanopillars is shown in Fig. 1(b), and a cross-sectional image in the inset (for $L = 150$ nm, also see Fig. S1) reveals the orientation of the Ag pillars. The SERS spectrum recorded from p-MA molecules chemisorbed from an atto molar (1 aM) concentration on Ag nanopillars is reported in Fig. 1(c). Several characteristic Raman modes of p-MA are clearly seen, highlighting the ultra-sensitive detection capability of the 3D Ag nanopillar structures.

3.2. Optical properties and SERS enhancement vs nanopillar length

Fig. 2(a) shows the reflectivity spectra of the planar Ag film with 150 nm thickness and Ag nanopillars with different *L* measured at room temperature in the spectral range between 250 nm and 800 nm. The planar Ag film shows high reflectivity in the visible-IR range and an absorption edge around 300 nm. The Ag nanopillars with $L = 150$ nm show a LSPR at 416 nm. By increasing *L* to 250 nm, an additional band appears at a wavelength of 350 nm, which is assigned to the cavity-enabled gap plasmons formed by the nanostructured arrays [3,5] and supported by the simulations presented below. When *L* is further increased to 350 nm, the cavity-enabled gap plasmon resonance mode becomes more pronounced, resulting in higher absorption in the ultraviolet range.

In order to investigate the sensing capability of these Ag nanopillars, SERS measurements (Fig. 2(b)) were carried out, where p-MA molecules at 1 μM concentration were chemisorbed onto the metal surfaces. The SERS spectrum for the 150 nm long Ag pillar structure (green trace-Fig. 2(b)) shows the characteristic Raman bands of p-MA molecule centered at 1077, 1143, 1183, 1310, 1390, 1434 and 1577 cm^{-1}. Their molecular vibrational assignments can be found elsewhere [8,58,59]. An increase in the pillar length leads to a significant enhancement of the Raman band intensities and signal-to-noise ratio (SNR). The inset shows the variation of the SERS signal intensity of the 1434 cm^{-1} band for 150–350 nm nanopillar lengths. An increasing SERS signal intensity with Ag pillar length is observed, where the nanopillar with $L = 350$ nm shows the highest SERS intensity of 110 kilo-counts. This can be ascribed to a decrement in the reflectivity of the Ag nanopillar with increasing *L* causing an increasing contribution of cavity resonances (Fig. 2(a)). The Raman spectrum (Fig. S2) measured for 3D Ag nanopillars prior to chemisorption of p-MA shows no Raman bands corresponding to any surface contamination, highlighting the fabrication quality of the nanopillars. The uniformity of the SERS signal enhancement is investigated by recording the spectra at different spatial (surface) locations (see Fig. S3), where the spectra show uniform signal intensities for the characteristic bands, including the high SNR band at 1434 cm^{-1}. The standard deviation is found to be less than 5%. An average SERS enhancement of 6×10^6 was obtained by evaluating the Raman band of p-MA at 1434 cm^{-1}using Ag pillars with $L = 350$ nm compared to the planar Ag film used as a reference (SERS enhancement factor calculation is shown in the Supporting Information).

The polarization-dependent optical properties and SERS enhancement are evaluated using the substrates with 250 nm long Ag nanopillars. Fig. 3(a) shows the reflectivity spectra of the samples measured with unpolarized, transverse magnetic (TM) and transverse electric (TE) polarized light. The spectra obtained using TM and TE modes clearly show the variation in the reflectivity, especially at a wavelength around the LSPR caused by the structural anisotropy originating from the nanopillar fabrication process. Fig. 3(b) shows the SERS spectra of the p-MA molecules chemisorbed at 1 μM concentration, obtained using TM and TE polarized light on Ag nanopillars with $L = 250$ nm. The SERS spectrum obtained using TM mode shows higher signal intensity compared to that of TE mode. These tendencies are further discussed using the simulation results presented below.

3.3. FDTD simulations: calculated reflectivity spectra, electric and magnetic field distributions

The obtained experimental results are supported by modeling of reflectivity of the Ag nanopillars with $L = 250$ nm using the finite-difference time-domain (FDTD) method. For that, an unit-cell of 2.8 $\times$ 4.5 μm^2 containing Ag nanopillars (as shown in Fig. 4(a)) was constructed and illuminated by x- or y- polarized plane waves. The simulated reflectivity presented in Fig. 4(b) is in good qualitative correspondence with the measured spectrum (Fig. 3(a)); however, a slight mismatch in the spectral positions of resonances and reflectivity values due to some deviations in shape, size and position of real pillars compared to those used in the model can be observed. To verify the experimentally obtained enhancement of the Raman signals, the electric and magnetic field distributions for several excitation wavelengths (350, 400 and 532 nm) are shown in Fig. 4(c,d). It can be seen that

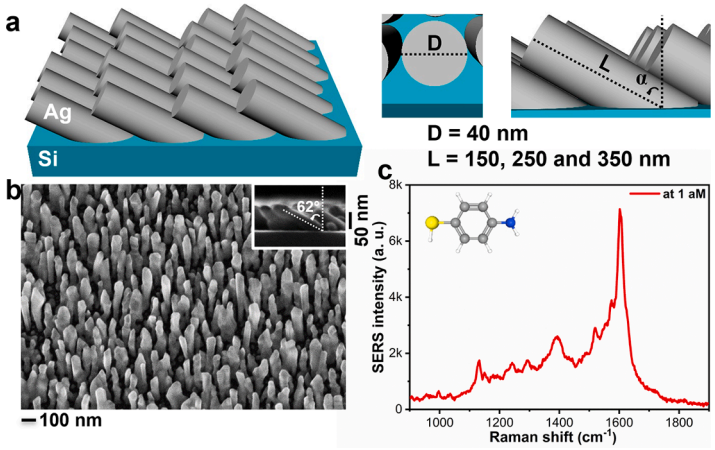

Fig. 1. (a) Schematic presentation of 3D Ag nanopillars. (b) Normal incidence SEM images of the 3D Ag nanopillar structures. The inset in (b) shows a cross-sectional view of the pillars for $L = 150$ nm. (c) SERS spectrum recorded from p-MA (chemisorbed from atto molar concentration solution) on Ag nanopillar structures. In the SERS measurement, an incident laser power of 22.25 μW and accumulation time of 10 s were used.

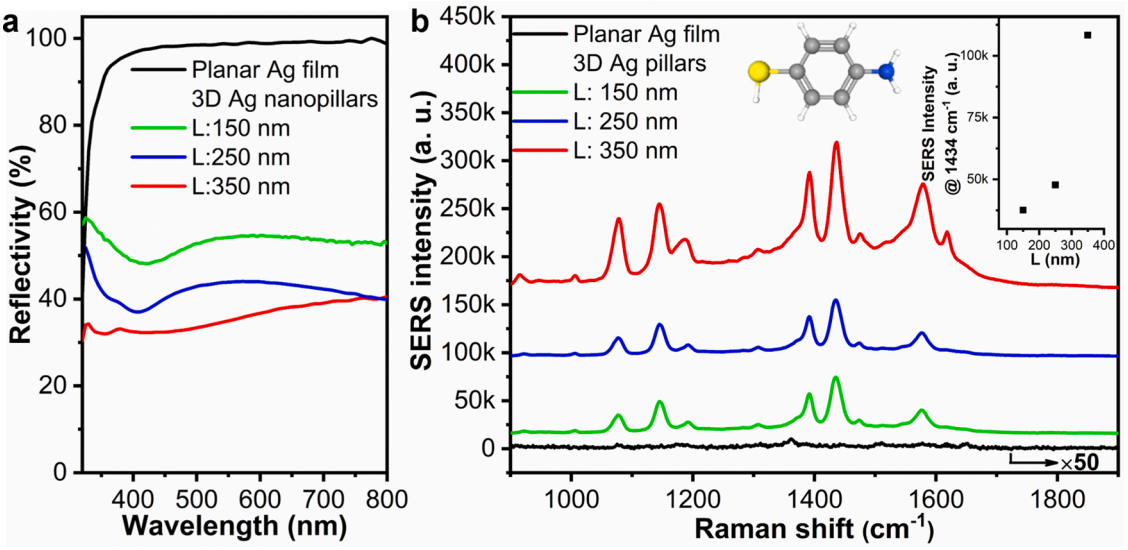

Fig. 2. (a) Experimental reflectivity spectra of planar Ag film and Ag nanopillar structures (with $L = 150$, 250 and 350 nm) obtained with unpolarized light source. (b) SERS spectra of p-MA chemisorbed at 1 μM concentration obtained from Ag film and Ag pillars of different L. The variation of the SERS band intensity at 1434 cm^{-1} for different L is shown in the inset. For all SERS measurements, an incident laser power of 0.45 mW and accumulation time of 30 s were used.

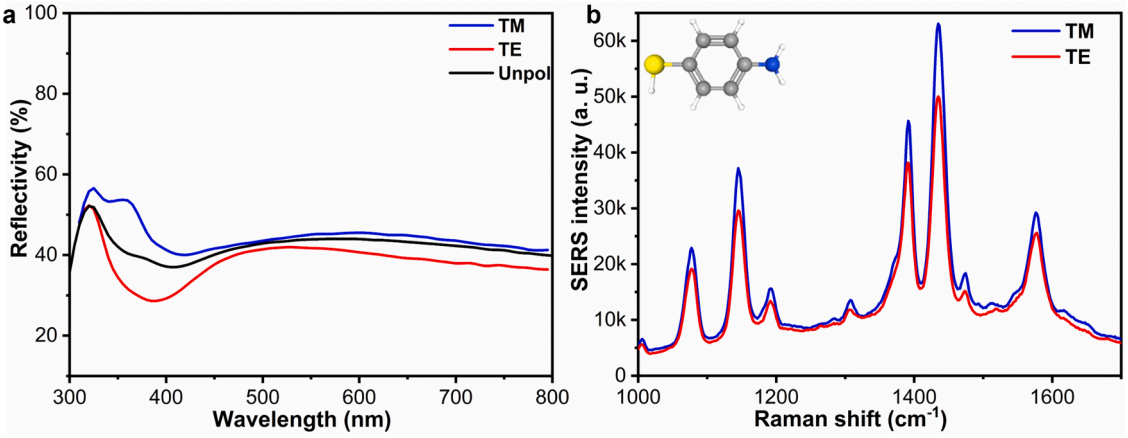

Fig. 3. (a) Experimental reflectivity spectra of Ag nanopillars ($L = 250$ nm) recorded with unpolarized as well as TM and TE polarized light. (b) SERS spectra of p-MA chemisorbed at 1 μM concentration recorded from Ag nanopillars ($L = 250$ nm) with incident TM and TE light polarizations. In the SERS measurements, an incident laser power of 0.45 mW and accumulation time of 30 s were used.

additionally to local fields formed at tops of the pillars the strong electric and magnetic fields are localized between them (in the cavity regions), resulting from the plasmonic resonances at the Ag/air interface. At an excitation wavelength of 350 nm, the fields are more intense for the *x*-polarized (TM) mode as the Ag nanopillars are much closer to each other (they are tilted in this direction, see Fig. 4(a)), which induces stronger near-field coupling and thus forms the lateral Ag/air/Ag cavities to localize and absorb the incident light. However, the electric field is not so well confined for the y- polarized (TE) light, resulting in the reflection variation. The Ag nanopillars exhibit similar tendencies in field distributions and reflectivities for other wavelengths (e.g., 400 and 532 nm). The TM mode at a wavelength of 532 nm (the one used in the experiments) shows much stronger local electromagnetic field confinement of hot-spots compared to TE mode (Fig. 4 (c and d)), which supports very well the polarization-dependent SERS measurements presented in Fig. 3 (b) where a high SERS signal enhancement is observed for TM polarized light.

3.4. The versatility of Ag nanopillars for sensing of different analytes, homogeneity and time stability of SERS spectra

The adaptability of 3D Ag nanostructures for bio/chemical sensing applications was demonstrated by testing various chemisorbed molecules. Fig. 5 shows SERS spectra obtained for p-MA, R6G and CV molecules on Ag nanopillars with $L = 350$ nm. All molecules show the spectra with high SNR for clearly distinguishable characteristic Raman bands: at 591, 674, 1188 and 1644 cm^{-1} for CV; at 773, 1362, 1510 and 1650 cm^{-1} for R6G; and at 1077, 1143, 1183, 1310, 1390, 1434 and 1577 cm^{-1} for p-MA showing good agreement with the literature [8,47, 60,61]. The Ag nanopillar substrates are found to provide a high uniformity of plasmonic properties, i.e. homogeneity of SERS spectra across large surface areas as can be seen in Supplementary, where Fig. S4 shows the Raman image for the intensity of R6G at 1650 cm^{-1} over nanopillar area of 150 × 90 μm^2.

According to the literature [62], Ag nanostructures can have a tendency to chemical degradation (oxidation) in ambient atmosphere. Therefore, chemical composition of the Ag substrates was tested using XPS: the spectra of as-grown nanostructures were compared with those

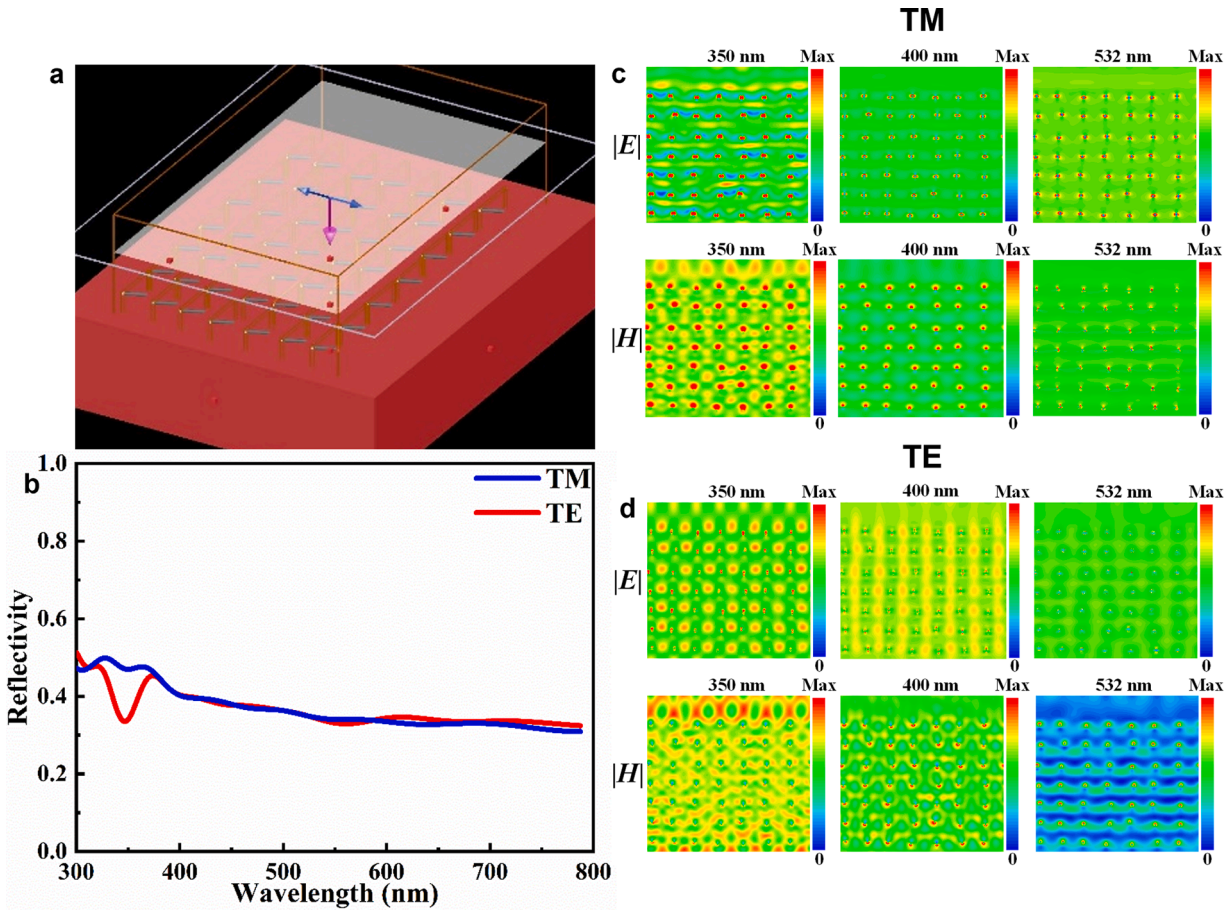

Fig. 4. (a) Unit cell of the 3D Ag nanopillars. (b) Calculated reflectivity spectra of the Ag nanopillars with $L = 250$ nm for TE and TM polarizations. (c and d) Electric and magnetic field distributions of Ag nanopillars ($L = 250$ nm) at the x-y plane for TM and TE polarizations, respectively.

for the samples stored in air for 1, 5 and 180 days. It is known that an oxide formation should lead to a small but detectable shift of the Ag 3d peaks. Indeed, a shift to lower binding energy for about 0.10–0.15 eV was observed after one day. However, keeping the samples in air for a longer period of up to 180 days did not result in further negative shifts (see Fig. S5). The XPS peak related to oxygen showed a small shoulder, which could be associated with Ag_2O formation, but its intensity did not show any considerable change with time. These data allow to conclude about a thin oxide shell formation after initial taking the samples from the vacuum into air but no oxidation on a long-time scale. These results are in good agreement with the earlier obtained ones in [30].

Growth of oxide can considerably affect the SERS performance of nanostructures, as for example was shown by Cheng et al. [63]. To study time stability of Raman spectra, SERS measurements were taken on Ag nanopillars (Fig. S6) after exposing the substrates to ambient air environment for 1, 5 and 180 days. Ag nanostructures showed excellent SERS signal reproducibility for the nanopillars kept in air up to 5 days. After keeping the sample for 180 days in ambient atmosphere, a significant reduction (15 ×) in the SERS signal intensity is noticed, which can be caused by the degradation of plasmonic properties due to other reasons than oxidation. No additional bands other than characteristic peaks of p-MA were observed in the spectra, i.e. indicating no surface contamination affecting the analyte detection.

3.5. Ultrasensitive detection of p-MA molecules

In order to investigate the high specificity and ultra-sensitivity, the SERS measurements were performed on Ag nanopillars with $L = 350$ nm, where p-MA molecules were chemisorbed at various concentrations. Fig. 6 shows the SERS signal intensity when the molecular concentration decreases from 1 μM to 1 aM. A decrease in the SERS signal intensity for the characteristic bands is observed with reducing the molecular concentration. More details on the relationship between the intensity of Raman bands and molar concentration of the analyte can be found in Supplementary (Fig. S7). However, several bands can still be well resolved for the lowest concentration of 1 aM level, which corresponds to very few or even a single molecule within the laser spot area. Moreover, deposition of p-MA at 1 aM concentration on several nanopillar substrates fabricated at identical conditions showed good reproducibility of the characteristic Raman bands (see Fig. S8). This very high sensitivity is realized due to the high density of hot-spots originated by the unique arrangement of the nanopillar arrays (high aspect ratio of 8.75 of individual pillars, good spatial separation from each other and a high degree of structural uniformity). Interestingly, at 1 μM concentration of p-MA, the Raman band at 1077 cm^{-1} corresponding to a1 mode of p-MA shows a high intensity, however, when decreasing the p-MA concentration this mode becomes undistinguishable. The SERS enhancement of a particular mode is highly dependent on the EM effect, and it is based on how the adsorbed p-MA molecule is oriented on the metal surface [59,64]. Nevertheless, at every concentration, the characteristic bands can be assigned to p-MA although there is a slight shift in the mode position.

Besides the ultra-sensing capability of the Ag nanopillars, reproducing the SERS signals with uniformity and molecular specificity is another critical factor for biosensing. To investigate that, SERS measurements for p-MA molecules (chemisorbed at 1 aM concentration) were performed at randomly selected spatial positions (within area of 4 cm^2) on the same substrate (Fig. 7). The SERS spectra show slight

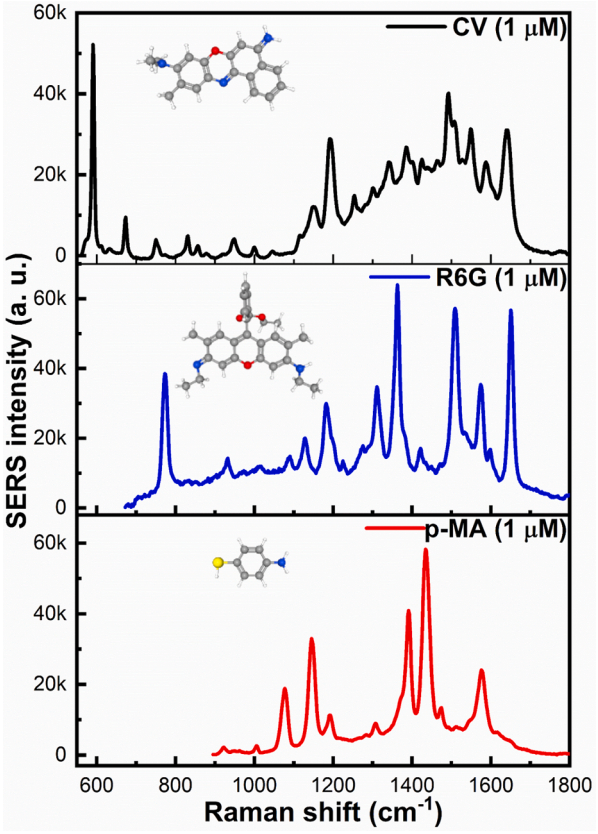

Fig. 5. SERS spectra recorded for various molecules chemisorbed from 1 μM solution on the Ag nanopillars with $L = 350$ nm. For CV and p-MA detection, an incident laser power of 0.45 mW and accumulation time of 10 s were used. For R6G analysis, an incident laser power of 22.25 μW and accumulation time of 10 s were used.

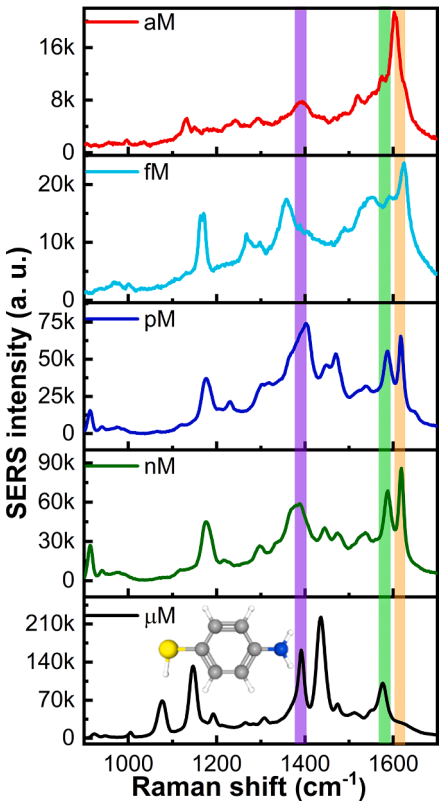

Fig. 6. SERS spectra recorded for p-MA molecules chemisorbed on Ag nanopillars of $L = 350$ nm at 1 μM, 1 nM, 1 pM, 1 fM and 1 aM concentrations. For all the SERS measurements, an incident laser power of 0.45 mW and accumulation time of 30 s were used.

variations in the band position and intensity, which can be ascribed to the orientation of the molecules that are adhered to the metal pillars at different locations. This tendency is well-known and typically observed at ultra-low molecular concentrations, particularly in the experiments of single molecule detection [65–67]. However, the characteristic Raman modes of p-MA are still clearly distinguishable in the obtained spectra despite the above-mentioned small shifts and intensity variation. The above-presented results on the achieved detection limits, reproducibility and uniformity of SERS spectra over large nanopillar areas as well as relative simplicity in fabrication demonstrate the state-of-the-art level of our SERS matrices. Indeed, attempts of other research groups to utilize GLAD technique for fabrication of substrates with Ag-based nanostructures for SERS showed much lower detection levels [46,68,69]. Use of other nanomaterials allows to obtain similar detection efficiency and reproducibility but, in many cases, the tedious and complicated fabrication steps limit their adaptability in practical applications, like, for example, for SERS substrates based on warped spaces reported by Mao et al. [25], 3D multilayered structures fabricated by Liu et al. [70], 3D nanohump arrays with Ag nanoparticles made by Li et al. [56], 3D nanolaminate plasmonic crystals coupled with Au nanoparticles according to Nam et al. [71], 3D Si nanopillar covered with Au nanoparticles and Ag nanosheets [72] and Ag nanoparticles decorated 3D sunflower nanoarrays [73].

3.6. Detection of analyte molecules using a portable handheld Raman spectrometer

To evaluate the applicability of the 3D Ag nanopillars for on-site diagnostics, a handheld Raman spectrometer is used to assess the substrates (see Fig. S9(b)). Fig. 8 shows the SERS spectra of p-MA molecules chemisorbed on Ag nanopillars with $L = 350$ nm at concentrations ranging from 1 μM down to 1 pM. At 1 μM concentration, the characteristic Raman bands of p-MA are clearly seen with a high SNR. The Raman bands at 1077 cm^{-1} and 1595 cm^{-1} show the highest intensities, and a few other low-intense bands are also observed. It is worth noticing that 1 μM p-MA spectrum (Fig. 6), measured using a stationary Raman spectrometer, shows strong Raman band intensities for 1143, 1390 and 1434 cm^{-1}. In the case of the handheld Raman spectrometer, Fig. 8, high intensity bands were observed at 1077 cm^{-1} and 1595 cm^{-1}. This difference is related to the dependence of the band intensity on the excitation wavelength [8,74,75]. For the stationary spectrometer, a 532 nm excitation laser source is used, whereas in the handheld Raman spectrometer, 785 and 853 nm lasers were used to acquire the spectra. After decreasing the molecular coverage to nM and pM levels, intensive Raman bands at 1077 cm^{-1} and 1595 cm^{-1} are still observed.

Further, the versatility of the 3D Ag nanopillars for handheld Raman spectrometer applications was evaluated using R6G molecules as analyte. The SERS spectra of R6G molecules chemisorbed at concentrations from 1 μM down to 1 fM on Ag nanopillars with $L = 350$ nm are shown in Fig. 9. Several characteristic Raman bands of R6G with a high SNR at 773, 1183, 1312, 1362 and 1510 cm^{-1} can be distinguished [8]. Albeit the fM concentration level, well distinguishable characteristic bands of R6G (with highest intensities at 1560 and 1609 cm^{-1} bands [47]) are distinctly noticed with the handheld Raman spectrometer.

3.7. Au nanopillars: fabrication, optical properties and Raman signal enhancement

In order to test other commonly used plasmonics materials, we have fabricated the nanopillars of Au with $D = 40$ nm, $\alpha = 62°$ and L of up to

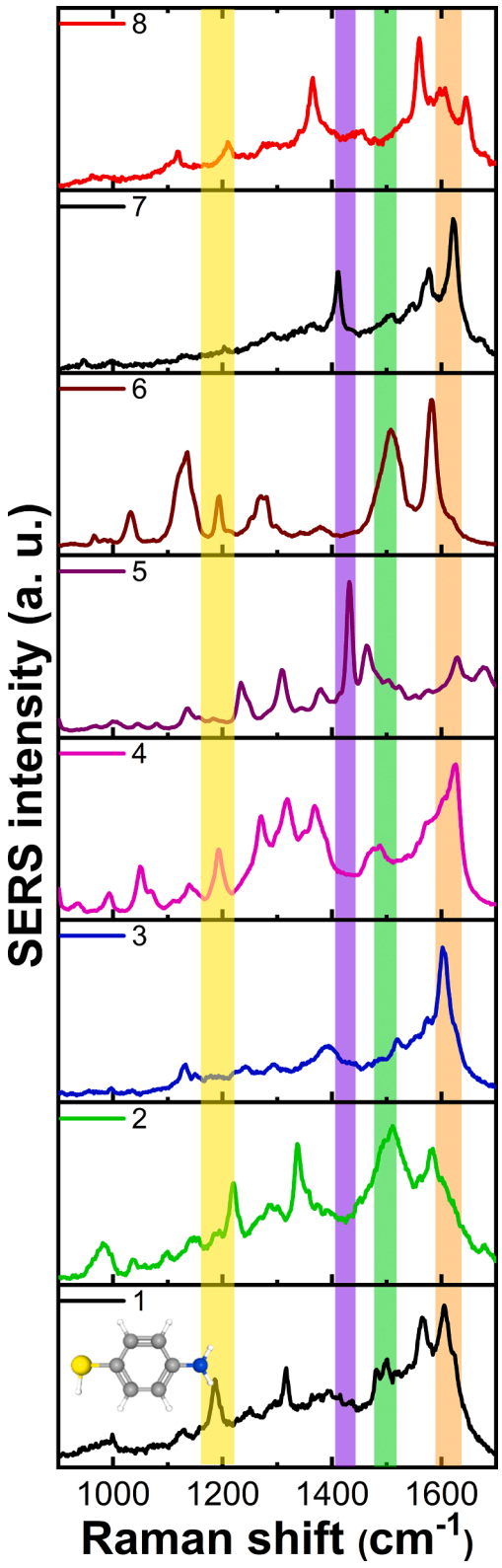

Fig. 7. SERS spectra of p-MA (at 1 aM concentration) recorded on 3D Ag nanopillars with L = 350 nm at 8 randomly selected positions of the same substrate, within area of 4 cm^2. An incident laser power of 22.25 μW and accumulation time of 10 s were used to acquire the SERS spectra.

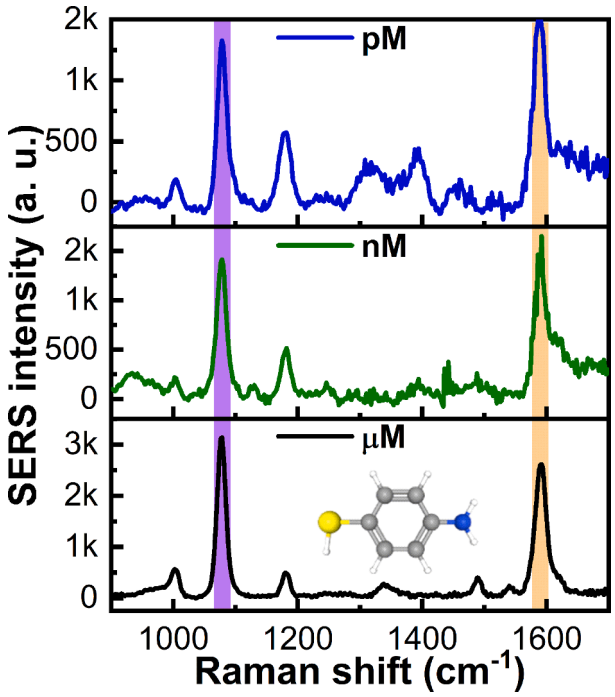

Fig. 8. SERS spectra of p-MA molecule, chemisorbed at concentrations ranging from 1 μM down to 1 pM, obtained on Ag nanopillars with L = 350 nm using a handheld Raman spectrometer.

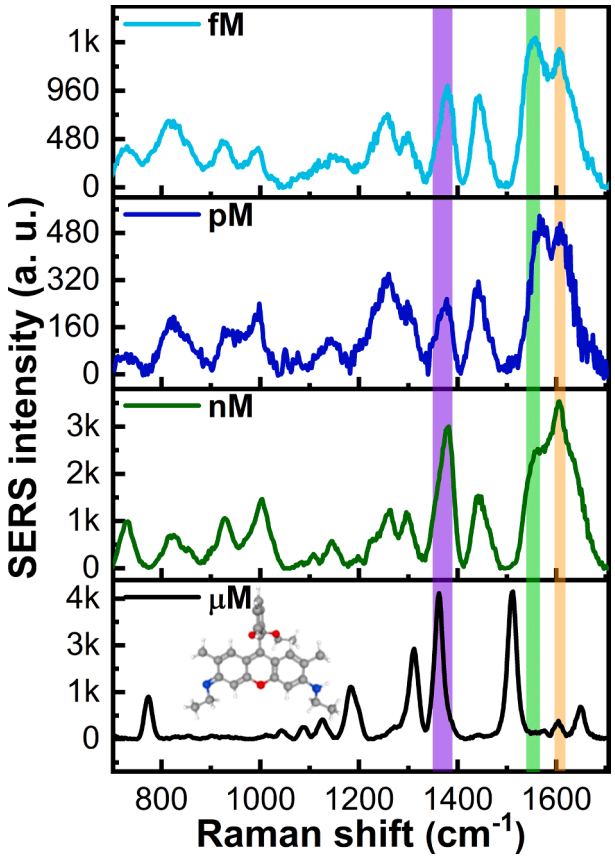

Fig. 9. SERS spectra of R6G molecule chemisorbed at various concentrations decreasing from 1 μM to 1 fM obtained on Ag nanopillars with L = 350 nm using a handheld Raman spectrometer.

350 nm using the same one-step oblique angle growth process. SEM image of the nanopillars with $L = 350$ nm is shown in the insert of Fig. 10 (a). The experimental reflectivity spectra of the 3D Au nanopillars are shown in Fig. 10(a). Similar to the Ag nanopillars case, a decrease in the reflectivity is observed with increasing the pillar length. The SERS spectra of R6G chemisorbed from 1 μM concentration on the substrates with various lengths of the nanopillars are shown in Fig. 10(b). Well distinguished Raman modes of R6G with a high SNR are clearly observed, particularly at 1362, 1510 and 1650 cm^{-1}. Similar to the case of silver, an increment of band intensities is observed with increasing the nanopillar length: Au nanopillars with $L = 350$ nm provide the highest signals.

Fig. 10(c) shows the SERS signal intensity variation at the 1362 cm^{-1} band position for different molecular concentrations. A decrease in the intensity is observed when the molecular concentration is reduced from μM to fM level but even at the lowest used concentration the characteristic bands can be registered with high SNR.

Homogeneity of the Raman signal enhancement was tested by recording the SERS spectra at various random positions on the same substrate. In Fig. 10(d), 50 SERS spectra of R6G obtained on the sample with 350 nm long nanopillars illustrate highly uniform and reproducible measurements. To demonstrate the potential of application of the Au nanopillars for on-site diagnostics, R6G molecules at various molecular concentrations (down to 1 fM) are tested with a handheld Raman spectrometer. The SERS spectra in Fig. S9 clearly show the prominent characteristic bands of R6G at 1362, 1560 and 1609 cm^{-1} with a high SNR at fM concentration. These results highlight the tremendous potential of the one-step fabrication of 3D nanopillars as a future prospect in ultra-sensitive SERS substrates.

4. Conclusions

In summary, we demonstrated a one-step scalable nanofabrication route to make uniform 3D Ag and Au nanopillar arrays on the macro-scale for SERS detection of the analyte molecules with concentrations as low as atto molar level. As shown by the modeling, this ultra-high detection capability was provided by hot-spot formation due to the coupling of LSPR from the nanopillars with the cavity-enabled gap plasmons. By increasing the nanopillar length up to 350 nm, a significant enhancement in the SERS signal intensity was obtained. 3D nanopillar arrays showed versatility in detecting various molecules typically used in SERS evaluations (CV, R6G and p-MA) at ultra-low concentrations. And for the first time, we showed that it was possible to use the developed substrates with nanopillars in a handheld Raman spectrometer to detect the analyte molecules at ultra-low concentrations of femto molar level. This work showed a clear perspective on the utilization of 3D nanopillar substrates for on-site diagnostics. The proposed SERS matrices with 3D nanopillars fabricated by a cost-effective one-step approach, choice of the appropriate metal, biocompatibility, and ultra-sensitive molecular detection capability, potentially open a new venue for ultra-sensitive SERS for recognition at single/a few molecule regimes.

CRediT authorship contribution statement

Anisha Chirumamilla: Methodology, Resources, Software,

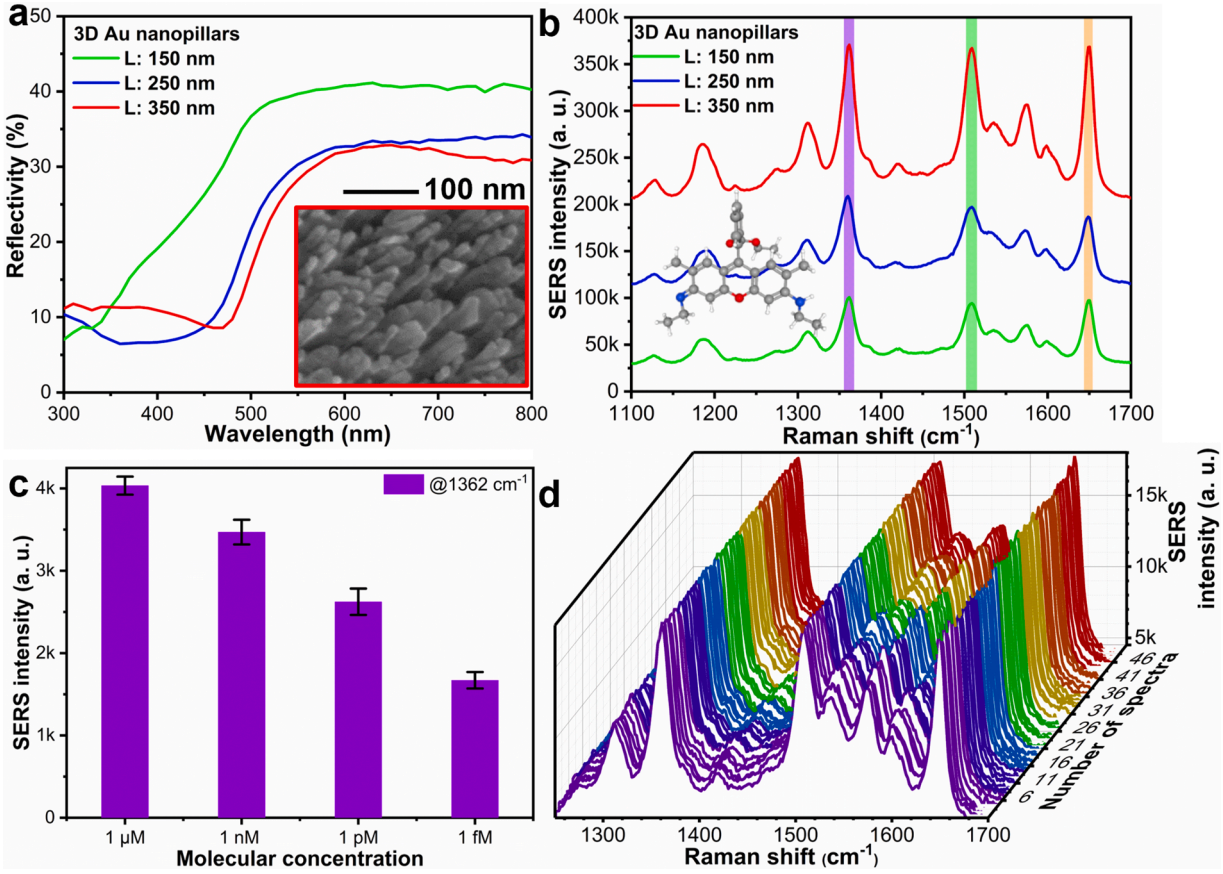

Fig. 10. (a) Experimental reflectivity spectra of Au nanopillar structures (with $L = 150$ nm, 250 nm and 350 nm) obtained with unpolarized light source. Inset shows the SEM image of the Au nanopillars with $L = 350$ nm. (b) SERS spectra of R6G chemisorbed at 1 μM concentration recorded on the Au nanopillars shown in (a), where the SERS measurements were carried out with an incident laser power of 22.25 μW and accumulation time of 10 s. (c) The variation of the band intensity at 1362 cm^{-1} for different molecular concentrations. (d) SERS spectra of R6G (at 1 μM concentration) recorded on Au nanopillars with $L = 350$ nm at 50 randomly selected points over area of 4 cm^2 of the same substrate. An incident laser power of 22.25 μW and accumulation time of 1 s were used to acquire the spectra.

Visualization, Formal analysis, Data curation, Writing – original draft. **Ioana-Malina Moise:** Methodology, Resources, Software, Visualization. **Ziru Cai:** Methodology, Resources, Software, Visualization. **Fei Ding:** Methodology, Resources, Software, Visualization. **Karina B. Jensen:** Methodology, Resources, Software, Visualization. **Deyong Wang:** Methodology, Resources, Software, Visualization. **Peter K. Kristensen:** Methodology, Resources, Software, Visualization. **Lars R. Jensen:** Methodology, Resources, Software, Visualization. **Peter Fojan:** Methodology, Resources, Software, Visualization. **Vladimir Popok:** Methodology, Resources, Software, Visualization, Conceptualization, Project administration, Supervision, Writing – review & editing. **Manohar Chirumamilla:** Conceptualization, Project administration, Supervision, Writing – review & editing. **Kjeld Pedersen:** Methodology, Resources, Software, Visualization, Conceptualization, Project administration, Supervision, Writing – review & editing.

Declaration of Competing Interest

The authors declare that they have no known competing financial interests or personal relationships that could have appeared to influence the work reported in this paper.

Data availability

No data was used for the research described in the article.

Acknowledgement

K. Pedersen, V. Popok and M. Chirumamilla acknowledge the financial support from the Novo Nordisk Foundation, grant number NNF20OC0064735.

Supplementary materials

Supplementary material associated with this article can be found, in the online version, at doi:10.1016/j.apmt.2023.101763.

References

[1] N.M. Ngo, M. Omidiyan, H.-.V. Tran, T.R. Lee, Stable Semi-Hollow Gold-Silver Nanostars with Tunable Plasmonic Resonances Ranging from Ultraviolet–Visible to Near-Infrared Wavelengths: implications for Photocatalysis, Biosensing, and Theranostics, ACS Appl. Nano Mater. 5 (2022) 11391.
[2] W. Hu, L. Xia, Y. Hu, G. Li, Recent progress on three-dimensional substrates for surface-enhanced Raman spectroscopic analysis, Microchem. J. 172 (2022), 106908.
[3] M. Chirumamilla, A. Chirumamilla, Y. Yang, A.S. Roberts, P.K. Kristensen, K. Chaudhuri, A. Boltasseva, D.S. Sutherland, S.I. Bozhevolnyi, K. Pedersen, Large-area ultrabroadband absorber for solar thermophotovoltaics based on 3D titanium nitride nanopillars, Adv. Opt. Mater. 5 (2017), 1700552.
[4] M. Chirumamilla, A.S. Roberts, F. Ding, D. Wang, P.K. Kristensen, S.I. Bozhevolnyi, K. Pedersen, Multilayer tungsten-alumina-based broadband light absorbers for high-temperature applications, Opt. Mater. Express 6 (2016) 2704.
[5] A. Chirumamilla, Y. Yang, M.H. Salazar, F. Ding, D. Wang, P.K. Kristensen, P. Fojan, S.I. Bozhevolnyi, D.S. Sutherland, K. Pedersen, M. Chirumamilla, Spectrally selective emitters based on 3D Mo nanopillars for thermophotovoltaic energy harvesting, Mater. Today Phys. 21 (2021), 100503.
[6] A.S. Roberts, M. Chirumamilla, D. Wang, L. An, K. Pedersen, N.A. Mortensen, S. I. Bozhevolnyi, Ultra-thin titanium nitride films for refractory spectral selectivity [Invited], Opt. Mater. Express 8 (2018) 3717.
[7] M. Chirumamilla, A. Chirumamilla, A.S. Roberts, R.P. Zaccaria, F. De Angelis, P. Kjær Kristensen, R. Krahne, S.I. Bozhevolnyi, K. Pedersen, A. Toma, Hot-spot engineering in 3D multi-branched nanostructures: ultrasensitive substrates for surface-enhanced Raman spectroscopy, Adv. Opt. Mater. 5 (2017), 1600836.
[8] A. Gopalakrishnan, M. Chirumamilla, F. De Angelis, A. Toma, R.P. Zaccaria, R. Krahne, Bimetallic 3D nanostar dimers in ring cavities: recyclable and robust surface-enhanced Raman Scattering substrates for signal detection from few molecules, ACS Nano 8 (2014) 7986.
[9] M. Chirumamilla, A. Toma, A. Gopalakrishnan, G. Das, R.P. Zaccaria, R. Krahne, E. Rondanina, M. Leoncini, C. Liberale, F. De Angelis, E. Di Fabrizio, 3D Nanostar dimers with a Sub-10-nm gap for single-/few-molecule surface-enhanced Raman scattering, Adv. Mater. 26 (2014) 2353.
[10] Q. Fu, Z. Li, F. Fu, X. Chen, J. Song, H. Yang, Stimuli-responsive plasmonic assemblies and their biomedical applications, Nano Today 36 (2021), 101014.
[11] B. Lv, H. Zhang, X. Zheng, H. Wang, W. Ge, Y. Ren, Z. Tan, M. Zhang, Z. Tang, Y. Liu, L. Zhang, Y. Wu, X. Jiang, W. Bu, Structure-oriented catalytic radiosensitization for cancer radiotherapy, Nano Today 35 (2020), 100988.
[12] W.Q. Lim, Z. Gao, Plasmonic nanoparticles in biomedicine, Nano Today 11 (2016) 168.
[13] T. Chen, H. Wang, G. Chen, Y. Wang, Y. Feng, W.S. Teo, T. Wu, H. Chen, Hotspot-induced transformation of surface-enhanced raman scattering fingerprints, ACS Nano 4 (2010) 3087.
[14] F.-.L. Zhang, J. Yi, W. Lin, E.-.M. You, J.-.S. Lin, H. Jin, W. Cai, Z.-.Q. Tian, J.-.F. Li, Gap-mode plasmons at 2nm spatial-resolution under a graphene-mediated hot spot, Nano Today 44 (2022), 101464.
[15] A. Alabastri, A. Toma, C. Liberale, M. Chirumamilla, A. Giugni, F. De Angelis, G. Das, E. Di Fabrizio, R.P. Zaccaria, Interplay between electric and magnetic effect in adiabatic polaritonic systems, Opt. Express 21 (2013) 7538.
[16] A.I. Pérez-Jiménez, D. Lyu, Z. Lu, G. Liu, B. Ren, Surface-enhanced Raman spectroscopy: benefits, trade-offs and future developments, Chem. Sci. 11 (2020) 4563.
[17] E. Cara, L. Mandrile, A. Sacco, A.M. Giovannozzi, A.M. Rossi, F. Celegato, N. De Leo, P. Hönicke, Y. Kayser, B. Beckhoff, D. Marchi, A. Zoccante, M. Cossi, M. Laus, L. Boarino, F. Ferrarese Lupi, Towards a traceable enhancement factor in surface-enhanced Raman spectroscopy, J. Mater. Chem. C 8 (2020) 16513.
[18] X. Wang, S.-.C. Huang, S. Hu, S. Yan, B. Ren, Fundamental understanding and applications of plasmon-enhanced Raman spectroscopy, Nat. Rev. Phys. 2 (2020) 253.
[19] Y. Wang, M. Zhang, Y. Lai, L. Chi, Advanced colloidal lithography: from patterning to applications, Nano Today 22 (2018) 36.
[20] Y. Liu, M. Kim, S.H. Cho, Y.S. Jung, Vertically aligned nanostructures for a reliable and ultrasensitive SERS-active platform: fabrication and engineering strategies, Nano Today 37 (2021), 101063.
[21] S. Habouti, M. Mátéfi-Tempfli, C.-.H. Solterbeck, M. Es-Souni, S. Mátéfi-Tempfli, M. Es-Souni, On-substrate, self-standing Au-nanorod arrays showing morphology controlled properties, Nano Today 6 (2011) 12.
[22] L. Guo, J.A. Jackman, H.-.H. Yang, P. Chen, N.-.J. Cho, D.-.H. Kim, Strategies for enhancing the sensitivity of plasmonic nanosensors, Nano Today 10 (2015) 213.
[23] Q. Tong, W. Wang, Y. Fan, L. Dong, Recent progressive preparations and applications of silver-based SERS substrates, TrAC Trends Anal. Chem. 106 (2018) 246.
[24] M. Yang, C. Wang, Y. Wei, C. Liu, F. Lei, X. Zhao, Z. Li, C. Zhang, J. Yu, Construct high-precise SERS sensor by hierarchical superhydrophobic Si/Cu(OH)2 platform for ultratrace detection of food contaminants, Sens. Actuators B 352 (2022), 131056.
[25] P. Mao, C. Liu, G. Favraud, Q. Chen, M. Han, A. Fratalocchi, S. Zhang, Broadband single molecule SERS detection designed by warped optical spaces, Nat. Commun. 9 (2018) 5428.
[26] L. Zhou, Y. Peng, N. Zhang, R. Du, R. Hübner, X. Wen, D. Li, Y. Hu, A. Eychmüller, Size-tunable gold aerogels: a durable and misfocus-tolerant 3d substrate for multiplex SERS detection, Adv. Opt. Mater. 9 (2021), 2100352.
[27] J. Yu, M. Yang, Z. Li, C. Liu, Y. Wei, C. Zhang, B. Man, F. Lei, Hierarchical particle-in-quasicavity architecture for ultratrace in situ raman sensing and its application in real-time monitoring of toxic pollutants, Anal. Chem. 92 (2020) 14754.
[28] M.E. Navarro-Segura, R.D. Rivera-Rangel, A. Arizmendi-Morquecho, I. López, J. Alvarez-Quintana, M. Sanchez-Dominguez, Ultra-high sensitivity surface-enhanced Raman spectroscopy (SERS) substrates based on au nanostructured hollow octahedra, Appl. Mater. Today 29 (2022), 101598.
[29] A. Sánchez-Iglesias, P. Aldeanueva-Potel, W. Ni, J. Pérez-Juste, I. Pastoriza-Santos, R.A. Alvarez-Puebla, B.N. Mbenkum, L.M. Liz-Marzán, Chemical seeded growth of Ag nanoparticle arrays and their application as reproducible SERS substrates, Nano Today 5 (2010) 21.
[30] S.M. Novikov, V.N. Popok, A.B. Evlyukhin, M. Hanif, P. Morgen, J. Fiutowski, J. Beermann, H.-.G. Rubahn, S.I. Bozhevolnyi, Highly stable monocrystalline silver clusters for plasmonic applications, Langmuir 33 (2017) 6062.
[31] C. Wang, M. Liu, Z. Wang, S. Li, Y. Deng, N. He, Point-of-care diagnostics for infectious diseases: from methods to devices, Nano Today 37 (2021), 101092.
[32] T.R. Alabi, D. Yuan, S. Das, Hierarchical metallic and ceramic nanostructures from laser interference ablation and block copolymer phase separation, Nanoscale 5 (2013) 3912.
[33] S. Jin, Z. Zhou, E.S.A. Sakr, M. Motlag, X. Huang, L. Tong, P. Bermel, L. Ye, G. J. Cheng, Scalable nanoshaping of hierarchical metallic patterns with multiplex laser shock imprinting using soft optical disks, Small 15 (2019), 1900481.
[34] H.-.K. Choi, S.-.M. Park, J. Jeong, H. Lee, G.J. Yeon, D.-.S. Kim, Z.H. Kim, Spatially controlled fabrication of surface-enhanced raman scattering hot spots through photoinduced dewetting of silver thin films, J. Phys. Chem. Lett. 13 (2022) 2969.
[35] J. Wu, X. Yang, J. Fang, Sensitive and reliable SERS substrates based on hierarchical nanoparticle arrays fabricated by confined spheroidization, Part. Part. Syst. Charact. 36 (2019), 1900268.
[36] C.V. Thompson, Solid-state dewetting of thin films, Annu. Rev. Mater. Res. 42 (2012) 399.
[37] S. Luo, A. Mancini, F. Wang, J. Liu, S.A. Maier, J.C. de Mello, High-Throughput Fabrication of Triangular Nanogap Arrays for Surface-Enhanced Raman Spectroscopy, ACS Nano 16 (2022) 7438.
[38] S. Augustine, M. Saini, S. KP, B.K. Parida, S. Hans, V. Pachchigar, B. Satpati, M. Ranjan, Au/Ag SERS active substrate for broader wavelength excitation, Opt. Mater. 135 (2023), 113319.

[39] Q. Zhang, Z. Liu, L. Duan, Z. Cao, B. Wu, L. Qu, C. Han, Ultrasensitive determination of lipid soluble antioxidants in food products using silver nano-tripod SERS substrates, Appl. Surf. Sci. 611 (2023), 155577.
[40] S.K. Srivastava, A. Shalabney, I. Khalaila, C. Grüner, B. Rauschenbach, I. Abdulhalim, S.E.R.S. Biosensor, Using metallic nano-sculptured thin films for the detection of endocrine disrupting compound biomarker vitellogenin, Small 10 (2014) 3579.
[41] H.-.H. Jeong, M.C. Adams, J.-.P. Günther, M. Alarcón-Correa, I. Kim, E. Choi, C. Miksch, A.F. Mark, A.G. Mark, P. Fischer, Arrays of plasmonic nanoparticle dimers with defined nanogap spacers, ACS Nano 13 (2019) 11453.
[42] A.G. Mark, J.G. Gibbs, T.-.C. Lee, P. Fischer, Hybrid nanocolloids with programmed three-dimensional shape and material composition, Nat. Mater. 12 (2013) 802.
[43] J.G. Gibbs, A.G. Mark, T.-.C. Lee, S. Eslami, D. Schamel, P. Fischer, Nanohelices by shadow growth, Nanoscale 6 (2014) 9457.
[44] Z.R. Lawson, A.S. Preston, M.T. Korsa, N.L. Dominique, W.J. Tuff, E. Sutter, J. P. Camden, J. Adam, R.A. Hughes, S. Neretina, Plasmonic gold trimers and dimers with air-filled nanogaps, ACS Appl. Mater. Interfaces 14 (2022) 28186.
[45] S. Camelio, D. Babonneau, E. Vandenhecke, G. Louarn, B. Humbert, Linear chains of Ag nanoparticles embedded in dielectric films for SERS applications in analytical chemistry, Nanoscale Adv 3 (2021) 6719.
[46] A. Rajput, S. Kumar, J.P. Singh, Vertically standing nanoporous Al–Ag zig-zag silver nanorod arrays for highly active SERS substrates, Analyst 142 (2017) 3959.
[47] Y.J. Liu, H.Y. Chu, Y.P. Zhao, Silver nanorod array substrates fabricated by oblique angle deposition: morphological, optical, and SERS characterizations, J. Phys. Chem. C 114 (2010) 8176.
[48] C.L. Leverette, S.A. Jacobs, S. Shanmukh, S.B. Chaney, R.A. Dluhy, Y.-.P. Zhao, Aligned silver nanorod arrays as substrates for surface-enhanced infrared absorption spectroscopy, Appl. Spectrosc. 60 (2006) 906.
[49] B. Li, T. Wang, Q. Su, X. Wu, P. Dong, Fabrication of au nanorods by the oblique angle deposition process for trace detection of methamphetamine with surface-enhanced raman Scattering, Sensors 19 (2019) 3742.
[50] R. Gao, Y. Zhang, F. Zhang, S. Guo, Y. Wang, L. Chen, J. Yang, SERS polarization-dependent effects for an ordered 3D plasmonic tilted silver nanorod array, Nanoscale 10 (2018) 8106.
[51] D. Bang, Y.W. Chang, J. Park, T. Lee, J. Park, J.-.S. Yeo, E.-.K. Kim, K.-.H. Yoo, Y.-. M. Huh, S. Haam, One-step electrochemical fabrication of vertically self-organized silver nanograss, J. Mater. Chem. A 1 (2013) 4851.
[52] J. Xiang, Y. Wang, Y. Wu, H. Fang, L. Shui, Z. Liu, T. Ding, Ordered hierarchical Ag nanostructures as surface-enhanced raman scattering platforms for (bio)chemical sensing and pollutant monitoring, ACS Appl. Nano Mater. 4 (2021) 11644.
[53] Y. Liu, M. Li, L. Liang, C. Feng, Y. Zhang, X. Liu, Y. Zhao, Effects of annealing temperature on morphological and optical properties of Ag nanoparticle array and its application in SERS, Opt. Mater. 128 (2022), 112381.
[54] F. Liu, B. Song, G. Su, O. Liang, P. Zhan, H. Wang, W. Wu, Y. Xie, Z. Wang, Sculpting extreme electromagnetic field enhancement in free space for molecule sensing, Small 14 (2018), 1801146.
[55] C. Yilmaz, A.E. Cetin, G. Goutzamanidis, J. Huang, S. Somu, H. Altug, D. Wei, A. Busnaina, Three-dimensional crystalline and homogeneous metallic nanostructures using directed assembly of nanoparticles, ACS Nano 8 (2014) 4547.
[56] Z. Li, G. Meng, Q. Huang, X. Hu, X. He, H. Tang, Z. Wang, F. Li, Ag Nanoparticle-grafted PAN-nanohump array films with 3D high-density hot spots as flexible and reliable SERS substrates, Small 11 (2015) 5452.
[57] B. Päivänranta, H. Merbold, R. Giannini, L. Büchi, S. Gorelick, C. David, J. F. Löffler, T. Feurer, Y. Ekinci, High aspect ratio plasmonic nanostructures for sensing applications, ACS Nano 5 (2011) 6374.
[58] J.B. Jackson, N.J. Halas, Surface-enhanced Raman scattering on tunable plasmonic nanoparticle substrates, Proc. Natl. Acad. Sci 101 (2004) 17930.
[59] M. Osawa, N. Matsuda, K. Yoshii, I. Uchida, Charge transfer resonance Raman process in surface-enhanced Raman scattering from p-aminothiophenol adsorbed on silver: Herzberg-Teller contribution, J. Phys. Chem. 98 (1994) 12702.
[60] M. Chirumamilla, A. Gopalakrishnan, A. Toma, R.P. Zaccaria, R. Krahne, Plasmon resonance tuning in metal nanostars for surface enhanced Raman scattering, Nanotechnology 25 (2014), 235303.
[61] G. Das, M. Chirumamilla, A. Gopalakrishnan, A. Toma, S. Panaro, R. Proietti Zaccaria, F. De Angelis, E. Di Fabrizio, Plasmonic nanostars for SERS application, Microelectron. Eng. 111 (2013) 247.
[62] Y. Han, R. Lupitskyy, T.-.M. Chou, C.M. Stafford, H. Du, S. Sukhishvili, Effect of oxidation on surface-enhanced Raman scattering activity of silver nanoparticles: a quantitative correlation, Anal. Chem. 83 (2011) 5873.
[63] Y.-.W. Cheng, C.-.W. Hsiao, C.-.H. Lin, L.-.Y. Huang, J.-.S. Chen, M.-.C. Yang, T.-. Y. Liu, Bionic 3D periodic nanostructures by Ag nano-islands deposited on cicada wings for rapid SERS detection, Surf. Coat. Technol. 436 (2022), 128323.
[64] M.R. Lopez-Ramirez, D. Aranda Ruiz, F.J. Avila Ferrer, S.P. Centeno, J.F. Arenas, J. C. Otero, J. Soto, Analysis of the potential dependent surface-enhanced Raman scattering of p-aminothiophenol on the basis of MS-CASPT2 calculations, J. Phys. Chem. C 120 (2016) 19322.
[65] H. Xu, E.J. Bjerneld, M. Käll, L. Börjesson, Spectroscopy of single hemoglobin molecules by surface enhanced Raman scattering, Phys. Rev. Lett. 83 (1999) 4357.
[66] H. Liu, L. Zhang, X. Lang, Y. Yamaguchi, H. Iwasaki, Y. Inouye, Q. Xue, M. Chen, Single molecule detection from a large-scale SERS-active Au79Ag21 substrate, Sci. Rep. 1 (2011) 112.
[67] G. Lu, B. Shrestha, A.J. Haes, Importance of tilt angles of adsorbed aromatic molecules on nanoparticle rattle SERS substrates, J. Phys. Chem. C 120 (2016) 20759.
[68] Y.-.J. Jen, W.-.C. Liu, M.-.Y. Cong, T.-.L. Chan, Bideposited silver nanocolloid arrays with strong plasmon-induced birefringence for SERS application, Sci. Rep. 10 (2020) 20143.
[69] Y. Liu, L. Ma, S. Zou, F. Zhao, Y. Wang, Y. Ling, Z. Zhang, Slanted Ag-Al alloy nanorods arrays for highly active and stable surface-enhanced Raman scattering substrates, Nanotechnology 30 (2019), 235703.
[70] H. Liu, C. Li, R. Song, S. Xu, A 3D mutilayer curved plasmonic coupling array with abundant and uniform hot spots for surface-enhanced Raman scattering, J. Phys. D 53 (2020), 055101.
[71] W. Nam, W. Kim, W. Zhou, E.-.A. You, A digital SERS sensing platform using 3D nanolaminate plasmonic crystals coupled with Au nanoparticles for accurate quantitative detection of dopamine, Nanoscale 13 (2021) 17340.
[72] X. He, Y. Liu, X. Xue, J. Liu, Y. Liu, Z. Li, Ultrasensitive detection of explosives via hydrophobic condensation effect on biomimetic SERS platforms, J. Mater. Chem. C 5 (2017) 12384.
[73] X. Zhang, X. Xiao, Z. Dai, W. Wu, X. Zhang, L. Fu, C. Jiang, Ultrasensitive SERS performance in 3D “sunflower-like” nanoarrays decorated with Ag nanoparticles, Nanoscale 9 (2017) 3114.
[74] K. Uetsuki, P. Verma, T.-a. Yano, Y. Saito, T. Ichimura, S. Kawata, Experimental identification of chemical effects in surface enhanced raman scattering of 4-aminothiophenol†, J. Phys. Chem. C 114 (2010) 7515.
[75] Y. Ward, R.J. Young, R.A. Shatwell, Effect of excitation wavelength on the Raman scattering from optical phonons in silicon carbide monofilaments, J. Appl. Phys. 102 (2007), 023512.